JOURNAL OF MATERIALS SCIENCE 27 (1992) 4489–4494

Abrasion-induced microstructural changes and material removal mechanisms in squeeze-cast aluminium alloy–silicon carbide composites

B. K. PRASAD, S. V. PRASAD*
Regional Research Laboratory, Hoshangabad Road, Habibganj Naka, Bhopal 462 026, India
A. A. DAS
Department of Manufacturing Engineering, Loughborough University of Technology, Loughborough, UK

An attempt has been made to understand wear-induced subsurface microstructural changes and material removal mechanisms in squeeze-cast BS LM11 alloy dispersed with 10 vol % SiC. Particles as well as fibres of SiC were separately dispersed in the alloy matrix to determine the influence of shape of the dispersoid on the abrasion behaviour of the latter. Abrasion tests were conducted on a standard rubber wheel abrasion test apparatus. Silica sand was used as the abrasive medium. Abrasive wear rates of the specimens were found to decrease gradually with the number of test intervals until a steady state value was attained. This was attributed to the protrusion of the reinforcement phase and abrasion-induced work hardening of the matrix in regions close to the abraded surface. The dispersoid/matrix interface as well as the shape of the dispersoid was found to influence the abrasion rate of the composites. A poor dispersoid/matrix interface led to higher rate of abrasion due to pull-out of the dispersoid. On the other hand, good bonding between the dispersoid and the matrix helped the dispersoid phase to be retained by the matrix, offering reduced rate of abrasion.

1. Introduction

Microstructures of materials used in applications requiring exceptional resistance to abrasion consist of hard second-phase particles in a relatively ductile matrix. Well-known examples are high-chromium white irons containing large volume fractions of M_7C_3-type carbides in an austenite or martensite matrix, and cobalt-based powder metallurgy alloys processed to produce carbides (stellites). In recent years, a number of aluminium alloy matrix composites with similar microstructures have been developed. Studies indicate that these lightweight composite materials have potential for applications subjected to abrasive wear conditions [1–7].

Abrasion resistance of a dual-phase material such as aluminium alloy–ceramic composites is mainly governed by the fracture of the hard ceramic phase which is generally brittle. The mode of fracture, in turn, is controlled by such factors as the size and shape of abrasive, its hardness relative to that of the second phase, load, and whether the abrasive is in the form of bonded sheet or loose particles. Abrasion resistance of hard particle composites has been measured by several investigators by use of a pin-on-drum apparatus with aloxide cloth sheet and the ASTM standard rubber wheel abrasion test (RWAT) apparatus with loose quartz abrasive particles. Material removal mechanisms have been studied with the help of scratch-test simulations. The effects of heat treatment on the abrasion of aluminium alloy matrix composites containing dispersions of SiC have also been investigated [8].

Banerjee *et al.* [6] measured the abrasive wear rates of a series of aluminium alloy–zircon particulate composites which contained a range of volume fractions of 100 μm zircon particles against aloxide cloth sheet using a pin-on-drum apparatus. Beyond a critical volume fraction of 0.09, abrasion resistance (inverse of the abrasive wear rate) was found to increase linearly with the volume fraction of zircon. These authors have also shown that the hard filler particles blunt the abrasive particles in the emery cloth sheet resulting in increased abrasion resistance of composites compared to base alloys as the number of passes on the same abrasive rises. Bhansali and Mehrabian [4] and Prasad *et al.* [2] have used the ASTM standard RWAT to characterize the low-stress abrasive wear behaviour of aluminium alloys. The abrasion rates of the alloys were found to decrease by a factor of five, due to dispersion of 0.35 V_f zircon or 0.2 V_f Al_2O_3. Interestingly, the abrasive wear rates of these composites (hardness 144 VHN) were lower than that of the 1020 steel and comparable to 1045 steel that was heat treated to a much higher hardness of 467 VHN.

* *Present address*: Materials Directorate (MLBT), Wright Laboratory, Wright-Patterson Airforce Base, OH 45433, USA.

0022–2461

It has been observed that wear-induced microstructural changes in regions close to wear surfaces play a significant role in governing the sliding wear resistance of materials [9–11]. Thus, although aluminium alloys dispersed with hard ceramics have tremendous potential in abrasive wear applications, limited information is available on their abrasive wear characteristics. Further, the nature of subsurface deformation during abrasion of aluminium alloys is not well understood.

In view of this, the present investigation was aimed at understanding the material removal mechanisms and subsurface deformation during low-stress abrasion of squeeze-cast BS LM11 alloy reinforced with 10 vol % SiC particles/fibres. The role of dispersoid/matrix interface on the abrasion resistance of the alloy was examined. Further, the base alloy also was subjected to identical tests to ascertain the influence of reinforcing SiC in the alloy.

2. Experimental procedure

2.1. Material preparation

BS LM11 (Al–4.5Cu–0.12Fe) alloy was chosen as the matrix. SiC particles (size 15–30 μm) and SiC fibres (length 3000 μm, diameter 10–15 μm) were used as reinforcements. Composites containing a random dispersion of 10 vol % each of the reinforcements separately, were prepared by the squeeze-casting technique. Detailed descriptions of material preparation are given elsewhere [12].

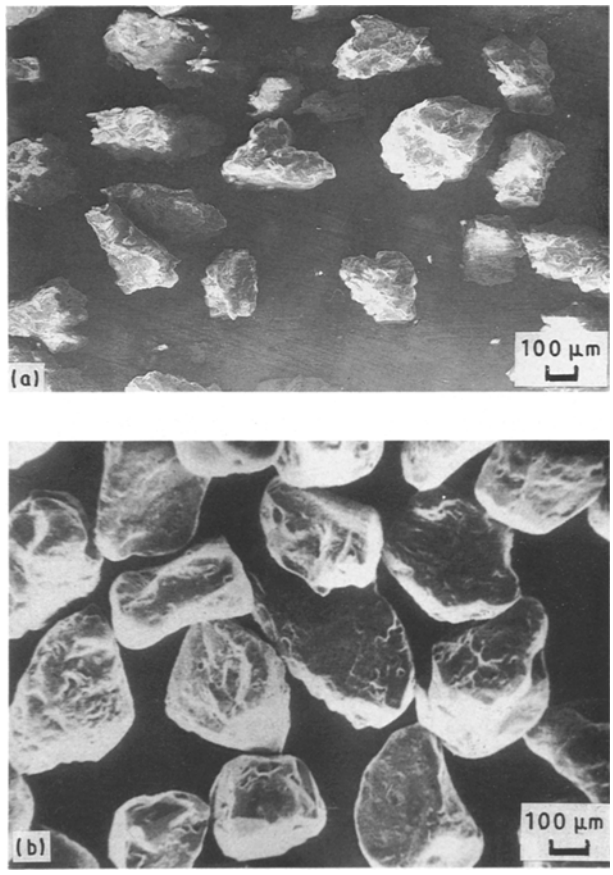

Figure 1 Scanning electron micrographs of silica sand: (a) angular particles used in the present investigation, and (b) semi-rounded particles specified by ASTM.

2.2. Abrasion test

Before commencement of the abrasion tests, specimens were metallographically polished. Low-stress abrasive wear tests were carried out using a Falex (USA) rubber wheel abrasion test (RWAT) apparatus as per ASTM G65-81 specifications [13] except that the shape of the silica sand used in the present study was angular (Fig. 1a) while ASTM specifies semi-rounded quartz particles (Fig. 1b). Briefly, the test consisted of gravity feeding of the abrasive particles (size 212–300 μm) between a rotating 20.3 cm diameter wheel rimmed with 1.27 cm thick chlorobutyl rubber (hardness Durometer A-60) and a rectangular test specimen (75 mm × 25 mm × 6 mm). The rotational speed of the wheel was 273 r.p.m.; the abrasive particle feed rate was 265 g min^{-1}, and the tests were conducted at applied loads of 22 and 49 N. Weight loss measurements were made at regular test intervals (each test interval corresponding to a sliding distance of 392 m) until a steady state wear loss was obtained. Tests from the second interval onwards were conducted on the same wear track, i.e. on pre-worn surfaces. Wear rates were calculated from weight loss measurements.

2.3. Microscopy

Specimens (8 mm × 8 mm × 6 mm) for microstructural investigations were prepared by standard metallographic techniques and etched with Keller's reagent. Metallographic specimens were examined using optical and scanning electron microscopy (SEM). Abraded surfaces were also examined in the SEM. Specimens after the abrasion test were sectioned perpendicular to the abraded surface, mounted in polyester resin, polished according to standard metallographic techniques and etched with Keller's reagent. Microhardness measurements were made on these transverse sections of the alloy as a function of depth below the abraded surface with the help of an optical microhardness tester. This was done to determine the work-hardening effect of the matrix due to abrasion. The transverse sections were also examined in the SEM to study the abrasion-induced microstructural changes in the subsurface regions. Specimens were sputtered with gold prior to the SEM examination.

3. Results

Fig. 2 shows the abrasive wear rates versus the number of test intervals at the applied loads of 22 and 49 N for the base alloy and the composites. It can be seen in the figure that increasing the applied load from 22 to 49 N led to an increase in the wear rate of the specimens by nearly three times. Further, the abrasive wear rate decreased initially with the number of test intervals and thereafter attained a steady state value. The extent of decrease was of the order of 40–60% (Fig. 2). The alloy dispersed with SiC particles showed the minimum wear rate while the base alloy suffered

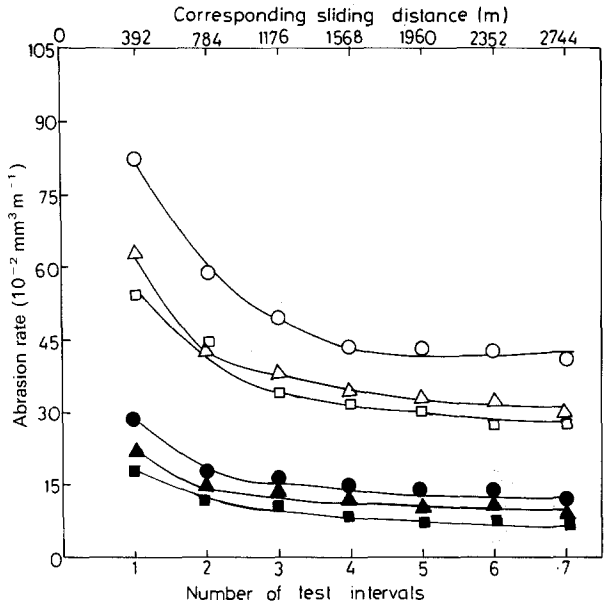

Figure 2 Abrasive wear rate of the base alloy and its composites containing SiC particles/fibres as a function of the number of test intervals. Applied load: (○, △, □) 49 N; (●, ▲, ■) 22 N, (○, ●) LM11, (△, ▲) LM11–SiC fibre, (□, ■) LM11–SiC particle.

from the maximum rate of wear. The wear rate of the composite containing SiC fibres was in between the two (Fig. 2). This trend was observed at both of the applied loads.

Scanning electron micrographs of the metallographically polished specimens of the alloy dispersed with SiC fibres and SiC particles revealing the distribution of the dispersoid phase in the matrix are shown in Fig. 3a and b, respectively.

Abraded surfaces of the SiC fibre composite showed a large number of fibre pull-outs at the higher load (Fig. 4a). However, at lower load, events of fibre pull-out in this composite were relatively less and some fibre protrusion was observed on the abraded surface (Figs 4b and c). Partial bonding of the dispersoid with the matrix may be noted in Fig. 4b while Fig. 4c (marked by arrow) reveals microcracks on a typical SiC fibre. On the other hand, the abraded surface of the alloy dispersed with SiC particles did not show particle pull-out to a significant extent, even at the higher load (Fig. 5a). There was, however, fracture and partial removal of SiC particles (Figs 5b and c, arrowed) during abrasion. A good particle/matrix interface in the abraded surface of this composite may be

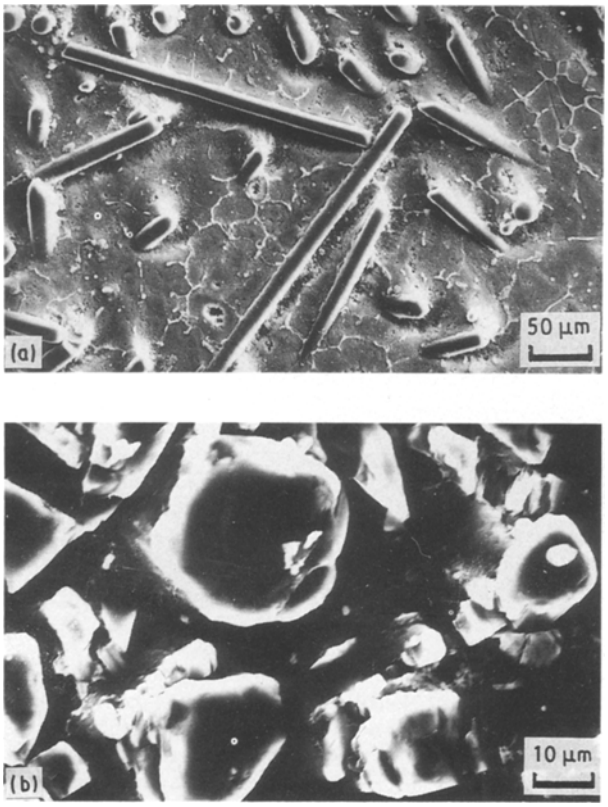

Figure 3 Scanning electron micrographs of metallographically polished surfaces of (a) LM11–SiC fibre, and (b) LM11–SiC particle composites.

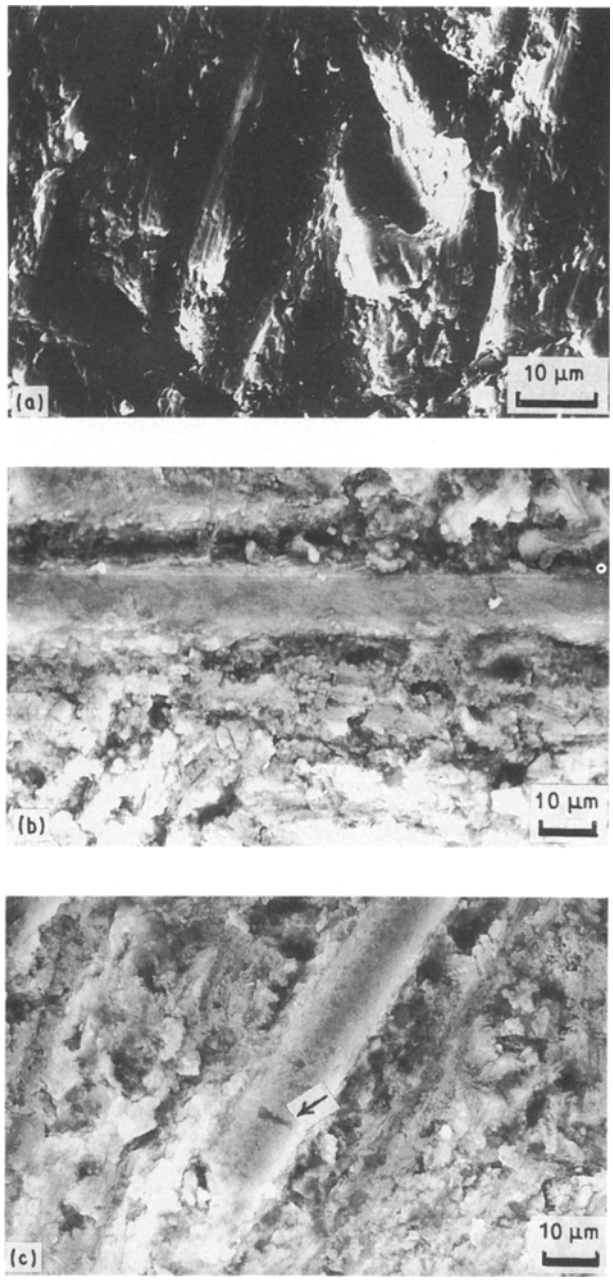

Figure 4 Abraded surfaces of the LM11–SiC fibre composite showing (a) pull-out of SiC fibres at 49 N, and (b, c) the protrusion of SiC fibres at 22 N. The weak fibre/matrix interface (b) and microcrack in a fibre generated during abrasion (c, arrowed) may be noted.

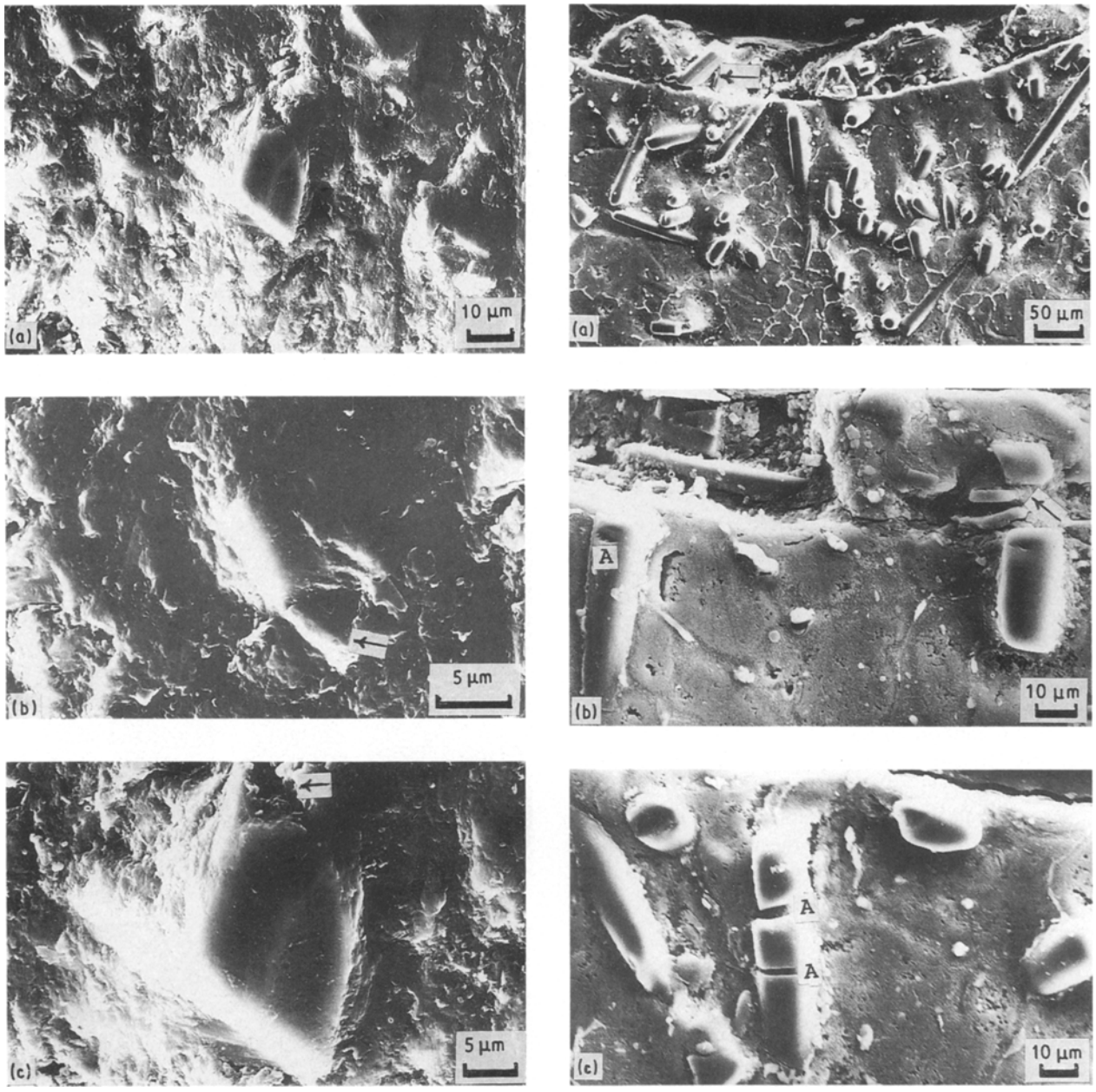

Figure 5 Abraded surfaces of the LM11–SiC particle composite showing (a) complete retention of the dispersoid particles during abrasion, and (b, c) pitting of a SiC particle (arrowed). A good particle/matrix interface may also be noted in (c). Applied load 49 N.

noted in Fig. 5c. Protrusion of the dispersoid on the abraded surface may also be noted in Fig. 5.

Fig. 6 shows the microstructure of the alloy reinforced with SiC fibres beneath the abraded surface. Cutting of the fibres leading to their fragmentation in the subsurface regions may be noted in Fig. 6a and b (arrowed). Fig. 6a also shows the continuous network of the $CuAl_2$ precipitate in the bulk (middle and bottom portions) and the broken precipitate network in the subsurface regions (top). The presence of microcracks in the SiC fibres in the subsurface regions may be seen in Fig. 6b and c (A). Broken precipitate particles in the subsurface regions may also be noted in Fig. 6b and c. Occasionally microcracks were observed in the subsurface regions (Fig. 6d).

Microhardness values of the matrix as a function of depth below the abraded surface may be seen in Fig. 7.

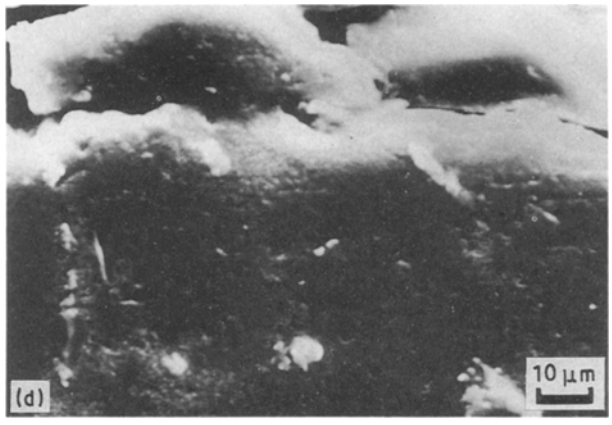

Figure 6 Scanning electron micrographs of transverse sections showing (a–d) abrasion-induced microstructural changes beneath the abraded surface. Note the decreasing extent of the break down of the $CuAl_2$ precipitate network with increasing depth below the abraded surface in (a) and the broken precipitate particles in the subsurface regions in (b) and (c). Arrows in (a) and (b) indicate fragmented pieces of SiC fibres in the subsurface regions. Microcracks in SiC fibres indicated by A in (b) and (c) were generated during abrasion. Occasional subsurface microcracks (d) were also observed. Applied load 49 N.

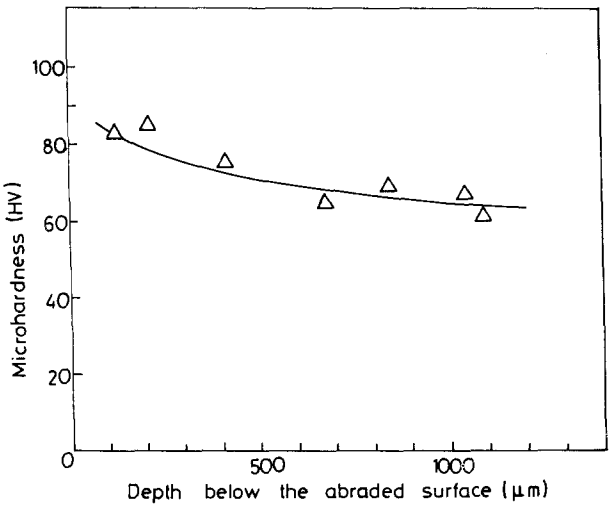

Figure 7 Microhardness of the matrix as a function of depth from the abraded surface. Applied load 49 N.

A higher hardness of the matrix close to the abraded surface, then in the bulk, may be noted in the figure. A typical microhardness indentation mark made in the regions close to the abraded surface is shown in Fig. 8.

4. Discussion

In the rubber wheel abrasion test, loose abrasive particles are fed between the specimen and rotating rubber wheel. When an abrasive particle encounters a hard dispersed particle/fibre, it can rise over the latter in response to greater hardness of the dispersoid. This gives rise to second-phase particle/fibre (SPP) protrusions (Figs 4b, c and 5). In the case of aluminium alloy composites containing high volume fractions (0.35 V_f) of hard zircon particles, the SPP protrusion has been found to protect the matrix completely from the action of the abrasive particles used in RWAT, until these hard particles are progressively removed by fracture [2]. The abrasive wear rates of these composites and those containing 20 vol% (0.20 V_f) alumina fibres, were comparable with those of normalized, quenched and tempered medium carbon steels and significantly less than that of low-carbon steel [2, 4]. However, in the present study, abrasive wear rates of composites ($25–35 \times 10^{-2}$ mm^3 m^{-1}) were found to be much higher than that of low-carbon steels (5.85×10^{-2} mm^3 m^{-1}) tested under identical conditions. This could be attributed to the low volume fraction of the hard phase (0.10 V_f). The interparticle/fibre spacing in the present case was too large to provide complete protection for the softer aluminium alloy matrix from the action of abrasive particles. However, partial protection provided by the hard SiC dispersoid in this case is evident from the relatively low abrasion rate of the composites, compared to the base alloy (Fig. 2).

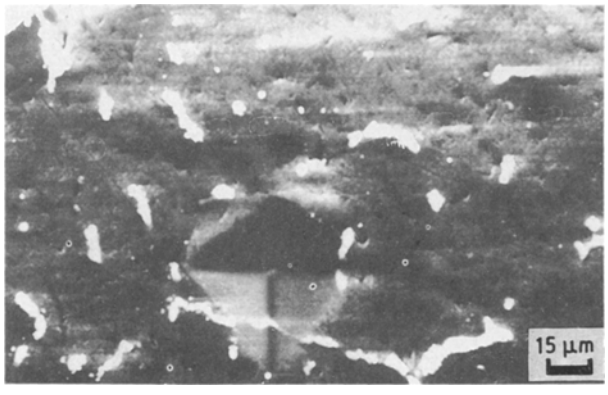

Figure 8 A typical microhardness indentation mark in the subsurface region. Note: the upper half of the mark closer to the abraded surface (top) is less than the lower half.

The abrasive wear rates were found to decrease progressively with increasing number of test intervals before a steady state value was recorded (Fig. 2). Because the starting surface was metallographically polished, the softer matrix is expected to be preferentially abraded in the beginning of the test. Further, with increase in the number of test intervals, more and more hard second-phase particles/fibres would protrude from the surface and thus offer protection to the latter. This may be one of the reasons for the observed decrease in abrasive wear rates with the number of test intervals (Fig. 2). Secondly, the matrix also became work hardened during the course of abrasion, as evinced by the identical wear behaviour of the base alloy (Fig. 2). Abrasion-induced subsurface matrix work hardening was also indicated by the difference in hardness between the bulk and that close to the abraded surface (Fig. 7). Microstructural investigations carried out on the transverse sections of the specimens also confirmed the work hardening of the matrix (Fig. 6). It is well known that the microstructure of a cast Al–4.5% Cu alloys consists of a $CuAl_2$ precipitate network in α-aluminium as can be seen in Fig. 6a (central and bottom regions). The network of $CuAl_2$ was completely broken down into small spherical particles in the subsurface regions (Fig. 6b, c), indicating heavy deformation of the latter [14]. Further, the extent of breaking of the network gradually decreased as the distance from the abraded surface increased (Fig. 6a). It is also interesting to note that the upper half of the hardness indentation mark closer to the abraded surface was less than the lower half, which is away from the abraded surface (Fig. 8), suggesting that the regions closer to the abraded surface were work hardened. Thus, the observations made in Figs 6 and 8 clearly indicate the work hardening of the subsurface regions during abrasion, as reflected in Fig. 7. Work hardening of steels during abrasion has also been reported earlier [15, 16]. In the present investigation, protrusion of hard particles/fibres and work hardening of the matrix during abrasion appeared to be responsible for the reduced abrasion rate with the number of test intervals (Fig. 2).

There appears to be a direct correlation between the observed abrasion rates and the particles (or the fibre)/matrix interface on the abraded surface. For example, the particle/matrix interface in the LM11–SiC particle composite appeared to be strong (Fig. 5c) and there were hardly any particle pull-outs (Fig. 5a). The abrasive wear rate of this composite was the lowest of all the three materials (Fig. 2) tested at

both loads. Removal of the SiC particle during abrasion appeared to be due to pitting (Fig. 5b and c, arrowed) probably caused by progressive fracture events. By contrast, the abraded surfaces of the alloys containing SiC fibres showed a considerable number of fibre pull-outs at higher load (Fig. 4a) leading to a higher rate of abrasion (Fig. 2). No significant fibre protrusions were observed in this case. However, at lower load, events of fibre pull-out were fewer in number and some fibre protrusion was observed (Fig. 4b, c). Microcracks on the SiC fibre in the abraded surface (Fig. 4c, arrowed) are formed by fine, sharp and angular abrasive particles and indicate the initial stage of fracture of the hard dispersoid phase [17]. Another important parameter in controlling the wear rate of the composites could be the shape of the dispersoid. It may be noted that the fibres had sharp tips. Such regions act as stress raiser points, thereby offering easy nucleation of cracks. The cracks would easily propagate via the poor fibre/matrix interface, ultimately leading to higher abrasion rates of the fibre composite. On the other hand, SiC particles having relatively smoother edges and sound interface with the matrix probably did not allow the microcracks to nucleate at, and propagate via, the particle/matrix interface as easily as in the case of the LM11–SiC fibre composite. The higher length-to-diameter (L/D) ratio of the SiC fibres also indicates increased probability of their fracture and partial removal than that of the smoother-edged particles. This explains the lowest wear rate of the composite containing SiC particles (Fig. 2).

5. Conclusions

1. The abrasive wear rates of the aluminium (LM11) alloy decreased in the presence of hard SiC dispersoid particles/fibres. This was due to the protection to the matrix offered by the SiC dispersoid against the abrasive medium.

2. The dispersoid/matrix interface and the shape of the dispersoid played an important role in governing the abrasive wear rate of the composites. Smoother edges of the SiC particles and a good particle/matrix interface in the SiC particle composite probably led to restricted nucleation and propagation of microcracks leading to a minimum rate of abrasion. On the other hand, the composite containing SiC fibres showed a higher wear rate than the former, which agreed well with the sharp tips of the SiC fibres and relatively poor fibre/matrix interface, both facilitating easy nucleation and propagation of microcracks leading to a faster rate of material removal.

3. In all cases, there was a progressive decrease in abrasion rate with the number of test intervals before the steady state values were recorded. This was attributed to the work hardening of the matrix and preferential removal of the matrix in the beginning of the test; the latter leading to a greater and greater number of dispersoid protrusions, offering an increasing extent of protection to the matrix.

4. Microstructural changes in the subsurface regions of the abraded surfaces indicated heavy deformation of the regions during abrasion. This was further supported by the abrasion-induced work hardening of the matrix evident from the increased hardness of the subsurface regions than the unaffected bulk matrix.

References

1. A. BANERJEE, S. V. PRASAD, M. K. SURAPPA and P. K. ROHATGI, *Wear* **82** (1982) 141.
2. S. V. PRASAD, P. K. ROHATGI and T. H. KOSEL, *Mater. Sci. Engng* **80** (1986) 213.
3. A. SATO and R. MEHRABIAN, *Metall. Trans.* **7B** (1976) 443.
4. K. J. BHANSALI and R. MEHRABIAN, *J. Metals* **32** (1982) 30.
5. M. K. SURAPPA, S. V. PRASAD and P. K. ROHATGI, *Wear* **77** (1982) 295.
6. A. BANERJEE, M. K. SURAPPA and P. K. ROHATGI, *Metall. Trans.* **14B** (1983) 273.
7. P. K. ROHATGI, B. C. PAI and S. C. PANDA, *J. Mater. Sci.* **14** (1979) 2277.
8. S. J. LIN and K. S. LIU, *Wear* **121** (1988) 1.
9. S. L. RICE, H. NOWOTNY and S. F. WAYNE, *Wear* **74** (1981) 131.
10. M. A. MOORE and R. M. DOUTHWAITE, *Met. Trans.* **7A** (1976) 1833.
11. D. A. RIGNEY and J. P. HIRTH, *Wear* **53** (1979) 345.
12. A. A. DAS, M. YACOUB, B. ZANTOUT and A. J. CLEGG, *Cast Metals* **1** (1988) 69.
13. "Standard practice for conducting dry sand/rubber wheel ASTM standard G65-81 abrasion tests" (American Society for Testing and Materials, Philadelphia, PA, 1981).
14. P. K. ROHATGI and B. C. PAI, *Wear* **28** (1974) 353.
15. K. M. MASHLOOSH and T. S. EYRE, *Tribo. Int.* **18** (1985) 259.
16. T. H. KOSEL and N. F. FIORE, "Abrasion in wear resistant steels", Final report to Decree and Company Centre, Department of Metallurgical Engineering and Materials Science, University of Notre Dame (1980).
17. S. V. PRASAD and T. H. KOSEL, *Wear* **95** (1984) 87.

Received 24 April
and accepted 5 August 1991